The 8th European Congress on Computational Methods in Applied Sciences and Engineering
ECCOMAS Congress 2022
5-–9 June 2022, Oslo, Norway

DESIGN OF PIEZOELECTRIC LATTICE METAMATERIALS

PAOLO BISEGNA, CLAUDIO INTRIGILA AND NICOLA A. NODARGI

Department of Civil Engineering and Computer Science
University of Rome Tor Vergata
via del Politecnico 1, 00133 Rome, Italy
e-mail: {bisegna,intrigila,nodargi}@ing.uniroma2.it

Key words: Piezoelectric materials, Metamaterials, Lattice materials, Homogenisation, Crystal networks, 3D-printing

Abstract. Piezoelectric lattice metamaterials are considered. A computationally-effective homogenisation method is developed based on the recent solution to the Saint-Venant problem for general anisotropic piezoelectric cylinders. A publicly available repository of unit cell topologies is used to identify piezoelectric metamaterials with optimal figures of merit.

1 INTRODUCTION

Piezoelectric materials find applications in many fields of science and technology, including sensors, actuators, energy harvesters and many other devices, owing to their ability to convert mechanical to electrical energy and vice versa. Their piezoelectric properties depend on their intrinsic crystallographic structures and compositions [1]. In order to enlarge the design space of piezoelectric properties, several piezoelectric materials have been thoroughly studied, including single crystals, ceramics, polymers, and a plethora of composites with different connectivity [2]. However, some restrictions still prevail [1].

In this paper, piezoelectric lattice metamaterials are explored (examples are shown in Figure 1). They are generated by the periodic repetition in space of a unit cell constituted by beams, whose cross section is assumed to be circular.

Piezoelectric metamaterials can be fabricated via 3D printing [1]. In fact, 3D printing of functionalised materials, like piezoelectric ones, is sometimes referred to as 4D printing. In [1], a photosensitive resin is used as bulk material, in which nanoparticles made of PZT, a piezoelectric ceramic, have been dispersed. Production of piezoelectric metamaterials is made in two steps. First, they are printed using high-resolution projected microstereolithography. Then, poling is performed, which is essential to reorganise and align the microscopic dielectric dipoles so that piezoelectric properties arise at the macroscale. As a consequence, the parent material turns out to be transversely isotropic, with the transverse isotropy axis coinciding with the poling direction.

The main features that determine the overall properties of piezoelectric lattice metamaterials include the unit cell topology and geometry, the relative density, and parent material properties. This work aims to devise a computationally-effective homogenisation method to provide the homogenised properties of piezoelectric lattice materials. In this regard, although the cylindrical

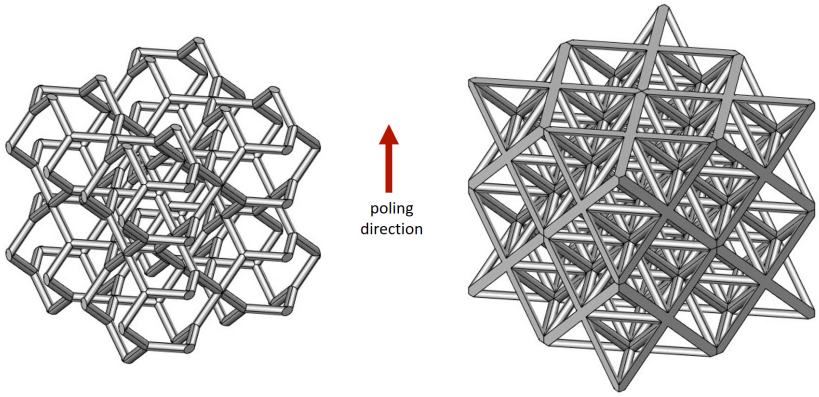

Figure 1: Examples of piezoelectric lattice metamaterials. $2 \times 2 \times 2$ tessellation at relative density $\bar{\rho} = 0.04$. On the left: pentamode unit cell (cub_Z03.6_R487). On the right: octet unit cell (cub_FZ12.0_E19) [4].

Table 1: Material properties in $\boldsymbol{e}$-form used in numerical applications [1]. Poling is along the x_3 axis.

C^E_{11} [GPa]	C^E_{12} [GPa]	C^E_{33} [GPa]	C^E_{13} [GPa]	C^E_{44} [GPa]	$\varepsilon^\epsilon_{11}/\varepsilon_0$ [-]	$\varepsilon^\epsilon_{33}/\varepsilon_0$ [-]	e_{31} [mC/m^2]	e_{33} [mC/m^2]	e_{15} [mC/m^2]
5.072	4.552	3.115	3.561	0.480	29.10	13.37	40.81	55.16	33.60

beams comprising the lattice are made of a transversely isotropic linear piezoelectric material, the transverse-isotropy axis of the material (i.e., the poling direction) does not generally coincide with the beam axis. Consequently, within the beam local reference frame, the piezoelectric constitutive law of the parent material is formulated as a general anisotropic constitutive law. Hence, instrumental in the homogenisation process are the results of the Saint-Venant problem for general anisotropic piezoelectric cylinders [3], enabling the usage of a very efficient beam model even for beams whose axis is oblique to the poling direction.

Finally, over 17,000 publicly available crystallographic network topologies [4] have been analyzed, regarded as cellular structures with nodes connected by piezoelectric beams [4], and structures with extremal piezoelectric properties are identified.

2 LINEAR PIEZOELECTRIC CONSTITUTIVE EQUATIONS

Denoting by $\boldsymbol{\epsilon}$, $\boldsymbol{\sigma}$, $\boldsymbol{E}$, and $\boldsymbol{D}$ respectively the (infinitesimal) strain, stress, electric field and electric displacement, the piezoelectric constitutive relationships can be expressed in four different forms, as follows [5]:

$$\begin{pmatrix} \boldsymbol{\sigma} \\ \boldsymbol{D} \end{pmatrix} = \begin{bmatrix} \mathbb{C}^{\boldsymbol{E}} & -\boldsymbol{e}^T \\ \boldsymbol{e} & \boldsymbol{\varepsilon}^{\boldsymbol{\epsilon}} \end{bmatrix} \begin{pmatrix} \boldsymbol{\epsilon} \\ \boldsymbol{E} \end{pmatrix}, \tag{1}$$

$$\begin{pmatrix} \boldsymbol{\epsilon} \\ \boldsymbol{D} \end{pmatrix} = \begin{bmatrix} \mathbb{S}^{\boldsymbol{E}} & \boldsymbol{d}^T \\ \boldsymbol{d} & \boldsymbol{\varepsilon}^{\boldsymbol{\sigma}} \end{bmatrix} \begin{pmatrix} \boldsymbol{\sigma} \\ \boldsymbol{E} \end{pmatrix}, \tag{2}$$

$$\begin{pmatrix} \boldsymbol{\epsilon} \\ \boldsymbol{E} \end{pmatrix} = \begin{bmatrix} \mathbb{S}^{\boldsymbol{D}} & \boldsymbol{g}^T \\ -\boldsymbol{g} & \beta^{\boldsymbol{\sigma}} \end{bmatrix} \begin{pmatrix} \boldsymbol{\sigma} \\ \boldsymbol{D} \end{pmatrix}, \tag{3}$$

$$\begin{pmatrix} \boldsymbol{\sigma} \\ \boldsymbol{E} \end{pmatrix} = \begin{bmatrix} \mathbb{C}^{\boldsymbol{D}} & -\boldsymbol{h}^T \\ -\boldsymbol{h} & \boldsymbol{\beta}^{\boldsymbol{\epsilon}} \end{bmatrix} \begin{pmatrix} \boldsymbol{\epsilon} \\ \boldsymbol{D} \end{pmatrix}. \tag{4}$$

Here $\mathbb{C}$, $\mathbb{S}$, $\boldsymbol{\varepsilon}$, and $\boldsymbol{\beta}$ respectively denote stiffness, compliance, electric permittivity, and electric impermeability tensors, the superscript ^{T} denotes transposition, and other superscripts denote the field which is held fixed (e.g., $\mathbb{C}^{\boldsymbol{E}}$ is the stiffness tensor at constant electric field). The third-order tensors $\boldsymbol{e}$, $\boldsymbol{d}$, $\boldsymbol{g}$, and $\boldsymbol{h}$ are piezoelectric tensors. The most relevant for applications are the $\boldsymbol{g}$ and $\boldsymbol{d}$ tensors. Equations (1)–(4) are denoted as $\boldsymbol{e}$-, $\boldsymbol{d}$-, $\boldsymbol{g}$-, and $\boldsymbol{h}$-form, respectively. They can be respectively derived by the following electro-elastic potentials:

$$\psi_{\mathrm{e}}(\boldsymbol{\epsilon}, \boldsymbol{E}) = \frac{1}{2}\left(\boldsymbol{\sigma}\cdot\boldsymbol{\epsilon} - \boldsymbol{D}\cdot\boldsymbol{E}\right) = \frac{1}{2}\left(\mathbb{C}^{\boldsymbol{E}}\boldsymbol{\epsilon}\cdot\boldsymbol{\epsilon} - 2\,\boldsymbol{e}\,\boldsymbol{\epsilon}\cdot\boldsymbol{E} - \boldsymbol{\varepsilon}^{\boldsymbol{\epsilon}}\boldsymbol{E}\cdot\boldsymbol{E}\right), \tag{5}$$

$$\psi_{\mathrm{d}}(\boldsymbol{\sigma}, \boldsymbol{E}) = \frac{1}{2}\left(\boldsymbol{\epsilon}\cdot\boldsymbol{\sigma} + \boldsymbol{D}\cdot\boldsymbol{E}\right) = \frac{1}{2}\left(\mathbb{S}^{\boldsymbol{E}}\boldsymbol{\sigma}\cdot\boldsymbol{\sigma} + 2\,\boldsymbol{d}\,\boldsymbol{\sigma}\cdot\boldsymbol{E} + \boldsymbol{\varepsilon}^{\boldsymbol{\sigma}}\boldsymbol{E}\cdot\boldsymbol{E}\right), \tag{6}$$

$$\psi_{\mathrm{g}}(\boldsymbol{\sigma}, \boldsymbol{D}) = \frac{1}{2}\left(\boldsymbol{\epsilon}\cdot\boldsymbol{\sigma} - \boldsymbol{E}\cdot\boldsymbol{D}\right) = \frac{1}{2}\left(\mathbb{S}^{\boldsymbol{D}}\boldsymbol{\sigma}\cdot\boldsymbol{\sigma} + 2\,\boldsymbol{g}\,\boldsymbol{\sigma}\cdot\boldsymbol{D} - \boldsymbol{\beta}^{\boldsymbol{\sigma}}\boldsymbol{D}\cdot\boldsymbol{D}\right), \tag{7}$$

$$\psi_{\mathrm{h}}(\boldsymbol{\epsilon}, \boldsymbol{D}) = \frac{1}{2}\left(\boldsymbol{\sigma}\cdot\boldsymbol{\epsilon} + \boldsymbol{E}\cdot\boldsymbol{D}\right) = \frac{1}{2}\left(\mathbb{C}^{\boldsymbol{D}}\boldsymbol{\epsilon}\cdot\boldsymbol{\epsilon} - 2\,\boldsymbol{h}\,\boldsymbol{\epsilon}\cdot\boldsymbol{D} + \boldsymbol{\beta}^{\boldsymbol{\epsilon}}\boldsymbol{D}\cdot\boldsymbol{D}\right). \tag{8}$$

In particular, ψ_{h} is the stored energy density for the piezoelectric continuum, whereas ψ_{e} is known as electromechanical enthalpy [5].

In [1] piezoelectric lattice metamaterials have been fabricated by additively manufacturing free-form, perovskite-based piezoelectric nanocomposites. The latter have been obtained by covalently bonding functionalized lead zirconate titanate (PZT) nanoparticle colloids with entrapped photo-active monomers. The as-fabricated nanocomposite system did not require post-heat treatment and achieved high structural fidelity and uniformity. Poling under a uniform electric field with standard corona poling method was performed in order to align the dipoles in the direction of the applied field. The material properties used in numerical applications are reported in Table 1 in the $\boldsymbol{e}$-form.

3 FIGURES OF MERIT

Figures of merit (FOMs) are combinations of material properties that characterize the performance of a piezoelectric material. FOMs are especially useful when different piezoelectric materials, composites, or lattices are to be compared. Several such FOMs, mainly based on the piezoelectric $\boldsymbol{d}$ and $\boldsymbol{g}$ constants, have been suggested [6, 7]. In this work, the following FOMs are considered, relevant to the longitudinal piezoelectric effect (Voigt notation is used and poling is along the x_3 axis):

- piezoelectric voltage coefficient g_{33}, relating the generated voltage to the stress applied along the transverse-isotropy axis; high values of g_{33} are especially beneficial for sensor applications;

- piezoelectric charge coefficient d_{33}, relating the induced strain to the electric field applied along the transverse-isotropy axis; high values of d_{33} are helpful for actuator applications;
- squared figure of merit $Q_{33}^2 = d_{33}\, g_{33}$; it is important in transmit-receive or pulse-echo systems and is used to characterise the sensor signal-to-noise ratio;
- electromechanical coupling factor $\kappa_{33} = d_{33}/(\varepsilon_{33}^{\sigma}\, s_{33}^{E})^{1/2}$ describe the effectiveness of the energy conversion due to the piezoelectric effect and is relevant in energy-harvesting applications;
- anisotropy factor $\zeta = d_{33}/\max\{|d_{31}|, |d_{32}|\}$ is relevant in transducers applications.

4 PIEZOELECTRIC BEAM CONSTITUTIVE RELATIONSHIPS

The Saint-Venant problem for general anisotropic linear piezoelectric cylinders was solved in [3] (see also [8, 9, 10, 11]). Under the assumption of material homogeneity along the cylinder axis, the Voigt hypothesis was shown to be a necessary condition for the solution, thus allowing for the reduction of the three-dimensional piezoelectric problem to a pair of uncoupled boundary-value problems on the cylinder cross section.

Let $\mathscr{B}$ be the cylinder, with bases Ω_0 and Ω_L. Let $(n_L,\, \boldsymbol{t}_L,\, m_L,\, \boldsymbol{m}_L, q_L)$ respectively denote the resultant axial force, shear force, torque, bending moment, and total free charge acting on Ω_L. Aiming at deriving the beam constitutive equations in terms of the stress and charge resultants $(n_L,\, \boldsymbol{t}_L,\, m_L,\, \boldsymbol{m}_L, q_L)$, the electro-elastic potential ψ_{g} (equation (7)) is computed in solution and integrated over the cylinder $\mathscr{B}$. It results to be a quadric form of those resultants and can be represented by:

$$\Psi_{\mathrm{g}} = \frac{1}{2}\left[(n_L,\, \boldsymbol{t}_L,\, m_L,\, \boldsymbol{m}_L)\cdot \boldsymbol{S}^q\,(n_L,\, \boldsymbol{t}_L,\, m_L,\, \boldsymbol{m}_L) - 2\, q_L\, \hat{\boldsymbol{g}}\cdot(n_L,\, \boldsymbol{t}_L,\, m_L,\, \boldsymbol{m}_L) - B^{\boldsymbol{r}} q_L^2\right], \quad (9)$$

where $\boldsymbol{S}^q$ is the open-circuit compliance matrix of the cylinder, $B^{\boldsymbol{r}}$ is the inverse capacitance of the free cylinder, and $\hat{\boldsymbol{g}}$ is its piezoelectric sensor vector. Those quantities were derived in closed form in the case of a homogenous cylinder with a circular cross section [3]. Basing on a customary energetic equivalence principle, the following definitions are introduced:

$$\left(\overline{\Delta w},\, \overline{\Delta \boldsymbol{u}},\, \overline{\Delta\theta},\, \overline{\Delta\boldsymbol{\vartheta}}\right) = \boldsymbol{S}^q\,(n_L,\, \boldsymbol{t}_L,\, m_L,\, \boldsymbol{m}_L) - \hat{\boldsymbol{g}}^T q_L\,, \quad (10)$$

$$\overline{\Delta V} = \hat{\boldsymbol{g}}\cdot(n_L,\, \boldsymbol{t}_L,\, m_L,\, \boldsymbol{m}_L) + B^{\boldsymbol{r}} q_L\,, \quad (11)$$

to be interpreted as the equivalent relative displacements ($\overline{\Delta w}$ and $\overline{\Delta \boldsymbol{u}}$, respectively dual to n_L and $\boldsymbol{t}_L$), the equivalent relative rotations ($\overline{\Delta\theta}$ and $\overline{\Delta\boldsymbol{\vartheta}}$, respectively dual to m_L and $\boldsymbol{m}_L$), and the equivalent electric potential difference ($\overline{\Delta V}$, dual to q_L) between the bases Ω_0 and Ω_L of the cylinder.

Equations (10)–(11) are the counterpart, at the beam level, of the general anisotropic linear constitutive law (3) at the material point level. They can be inverted, yielding:

$$(n_L,\, \boldsymbol{t}_L,\, m_L,\, \boldsymbol{m}_L) = \boldsymbol{K}^V\left(\overline{\Delta w},\, \overline{\Delta \boldsymbol{u}},\, \overline{\Delta\theta},\, \overline{\Delta\boldsymbol{\vartheta}}\right) + \hat{\boldsymbol{e}}^T\overline{\Delta V}, \quad (12)$$

$$q_L = -\hat{\boldsymbol{e}}\cdot\left(\overline{\Delta w},\, \overline{\Delta \boldsymbol{u}},\, \overline{\Delta\theta},\, \overline{\Delta\boldsymbol{\vartheta}}\right) + C^s\overline{\Delta V}, \quad (13)$$

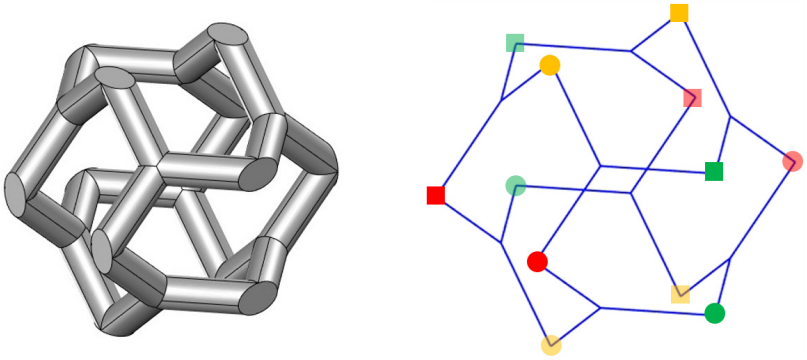

Figure 2: Example of a periodic unit cell (labelled cub_Z03.6_R487 in [4]). On the left: 3D model. On the right: beam model. Corresponding nodes on opposite faces of the periodic unit cell are denoted by markers of the same shape and colour.

where $\boldsymbol{K}^V$ is the closed-circuit stiffness matrix of the cylinder, C^s is the capacitance of the clamped cylinder, and $\hat{\boldsymbol{e}}$ is its piezoelectric $\boldsymbol{e}$-vector.

The equivalent relative displacements and rotations $(\overline{\Delta w}, \overline{\Delta \boldsymbol{u}}, \overline{\Delta \theta}, \overline{\Delta \boldsymbol{\vartheta}})$ are then expressed as functions of the displacements $\boldsymbol{s}$ of the cylinder bases (3 translations and 3 rotations for each base). Analogously, the equivalent electric potential difference ΔV is expressed as a function of the electric potentials $\boldsymbol{V}$ of the cylinder bases (one for each base). Moreover, the force and couple resultants $(n_L, \boldsymbol{t}_L, m_L, \boldsymbol{m}_L)$, together with the analogues resultants acting on the base Ω_0 obtained by equilibrium of $\mathscr{B}$, are collected into the 12-component force vector $\boldsymbol{f}$, and the total free charge q_L, together with the total free charge q_0 obtained by charge balance, are collected into the 2-component vector $\boldsymbol{q}$. Accordingly, equations (12)–(13) is transformed into:

$$\begin{pmatrix} \boldsymbol{f} \\ \boldsymbol{q} \end{pmatrix} = \begin{bmatrix} \tilde{\boldsymbol{K}}^V & -\tilde{\boldsymbol{e}}^T \\ -\tilde{\boldsymbol{e}} & -\tilde{\boldsymbol{C}}^{\boldsymbol{s}} \end{bmatrix} \begin{pmatrix} \boldsymbol{s} \\ -\boldsymbol{V} \end{pmatrix}, \tag{14}$$

Equation (14) relates the force vector $\boldsymbol{f}$ and the total free charge vector $\boldsymbol{q}$ on the cylinder bases to the displacements $\boldsymbol{s}$ and the electric potentials $\boldsymbol{V}$ of the cylinder bases. It yields the stiffness matrix of a piezoelectric beam made of a fully anisotropic piezoelectric material. Accordingly, the electromechanical enthalpy Ψ_{e} of the piezoelectric beam, to be used in the homogenisation process, is given by:

$$\Psi_{\mathrm{e}} = \frac{1}{2}\left(\boldsymbol{f}\cdot\boldsymbol{s} - \boldsymbol{q}\cdot\boldsymbol{V}\right) = \frac{1}{2}\begin{pmatrix} \boldsymbol{s} \\ -\boldsymbol{V} \end{pmatrix}^T \begin{bmatrix} \tilde{\boldsymbol{K}}^V & -\tilde{\boldsymbol{e}}^T \\ -\tilde{\boldsymbol{e}} & -\tilde{\boldsymbol{C}}^{\boldsymbol{s}} \end{bmatrix} \begin{pmatrix} \boldsymbol{s} \\ -\boldsymbol{V} \end{pmatrix}. \tag{15}$$

5 HOMOGENISATION

The homogenised constitutive properties of periodic composite materials can be computed by classical asymptotic homogenisation [12]. This method has a rigorous mathematical foundation and requires the solution to the cell problem formulated on the periodic unit cell of the material under periodic boundary conditions. Asymptotic homogenisation of periodic piezoelectric com-

posites has been reported, e.g., in [13, 14, 15]. Therein the unit cell problem was numerically solved using solid elements at the expense of a relatively high computational cost.

For periodic lattice metamaterials, especially at low relative densities, it would be convenient to regard the periodic unit cell as a system of beams. For elastic lattices, that point of view was shared, e.g., in [16, 4]. It is here first adopted for lattices made of a poled piezoelectric parent material.

The $\boldsymbol{e}$-form of the homogenised constitutive equations, taking the strain and the electric field as independent variables, is derived. To this end, a macroscale homogeneous strain $\overline{\boldsymbol{\epsilon}}$ and electric field $\overline{\boldsymbol{E}}$ are applied to the unit cell. Then, the total electromechanical enthalpy of the unit cell is computed as the sum of the electromechanical enthalpy of every single beam, which in turn descends from equation (15). Finally, the unit cell problem is solved by taking the stationary condition of the total electromechanical enthalpy with respect to nodal displacements, rotations and electric potentials, under periodic boundary conditions. The solution to the unit-cell problem is carried out in the fashion of a standard finite element analysis of a system of beams. Periodicity constraints are imposed on corresponding nodes located on opposite faces of the unit cell, as shown in Figure 2. As a result, the homogenised electromechanical enthalpy density is obtained, yielding the homogenised constitutive matrix of the lattice in $\boldsymbol{e}$-form. In formulas, the homogenisation procedure is formulated as follows:

$$\psi_{\mathrm{e}}^{\mathrm{hom}}(\overline{\boldsymbol{\epsilon}},\overline{\boldsymbol{E}}) = \frac{1}{2}\begin{pmatrix}\overline{\boldsymbol{\epsilon}}\\ \overline{\boldsymbol{E}}\end{pmatrix}^T\begin{bmatrix}\overline{\mathbb{C}}^{\boldsymbol{E}} & -\overline{\boldsymbol{e}}^T\\ -\overline{\boldsymbol{e}} & -\overline{\boldsymbol{\varepsilon}}^{\boldsymbol{\epsilon}}\end{bmatrix}\begin{pmatrix}\overline{\boldsymbol{\epsilon}}\\ \overline{\boldsymbol{E}}\end{pmatrix} = \frac{1}{|\mathcal{U}|}\underset{\substack{\{\boldsymbol{s},\boldsymbol{V}\}\\ \mathcal{P}}}{\mathrm{stat}}\sum_b \frac{1}{2}\begin{pmatrix}\boldsymbol{s}_b\\ -\boldsymbol{V}_b\end{pmatrix}^T\begin{bmatrix}\tilde{\boldsymbol{K}}_b^V & -\tilde{\boldsymbol{e}}_b^T\\ -\tilde{\boldsymbol{e}}_b & -\tilde{\boldsymbol{C}}_b^{\boldsymbol{u}}\end{bmatrix}\begin{pmatrix}\boldsymbol{s}_b\\ -\boldsymbol{V}_b\end{pmatrix}, \tag{16}$$

where $|\mathcal{U}|$ is the unit cell volume, and the sum at the right-hand side is extended over the beams comprising the unit cell. Of course, a standard assembly procedure guarantees that beams converging into a node share the same nodal degrees of freedom. In passing, it is noted that only one of two corresponding beams on opposite boundaries of the unit cell should be considered. The periodic boundary conditions $\mathcal{P}$ are formulated as follows, for any couple (i,j) of corresponding nodes on opposite boundaries of the unit cell (Figure 2):

$$\mathcal{P}\colon \boldsymbol{u}_j = \boldsymbol{u}_i + \overline{\boldsymbol{\epsilon}}[\boldsymbol{x}_j - \boldsymbol{x}_i]\,, \quad \boldsymbol{\varphi}_j = \boldsymbol{\varphi}_i\,, \quad V_j = V_i - \overline{\boldsymbol{E}}[\boldsymbol{x}_j - \boldsymbol{x}_i], \tag{17}$$

with $\boldsymbol{u}_i$ and $\boldsymbol{\varphi}_i$ respectively denoting the displacements and rotations of node i, and $\boldsymbol{s}_i = (\boldsymbol{u}_i;\boldsymbol{\varphi}_i)$. The contribution $\varepsilon_0\|\boldsymbol{E}\|^2/2$, where ε_0 denotes the vacuum permittivity and $\|\cdot\|$ is the norm, is added to the homogenised electromechanical enthalpy density $\psi_{\mathrm{e}}^{\mathrm{hom}}$, in order to account for the electric field contribution in the free space of the lattice, which may be significant at low relative density values [17].

By taking the derivative of the homogenised electromechanical enthalpy density $\psi_{\mathrm{e}}^{\mathrm{hom}}$ with respect to $\overline{\boldsymbol{\epsilon}}$ and $\overline{\boldsymbol{E}}$, the homogenised constitutive relationships are obtained. Specifically, those equations describe the average stress $\overline{\boldsymbol{\sigma}}$ and (the opposite of) the average electric displacement $\overline{\boldsymbol{D}}$ arising in the metamaterial due to the application of a strain field and an electric field with prescribed averages $\overline{\boldsymbol{\epsilon}}$ and $\overline{\boldsymbol{E}}$, respectively. Because the homogenised constitutive equations result to be linear, nine independent loading conditions are required for their complete characterization. In practice, the macroscale homogeneous strain or electric fields are applied component-wise to the unit cell. Each load case yields a column of the homogenised constitutive matrix. Finally,

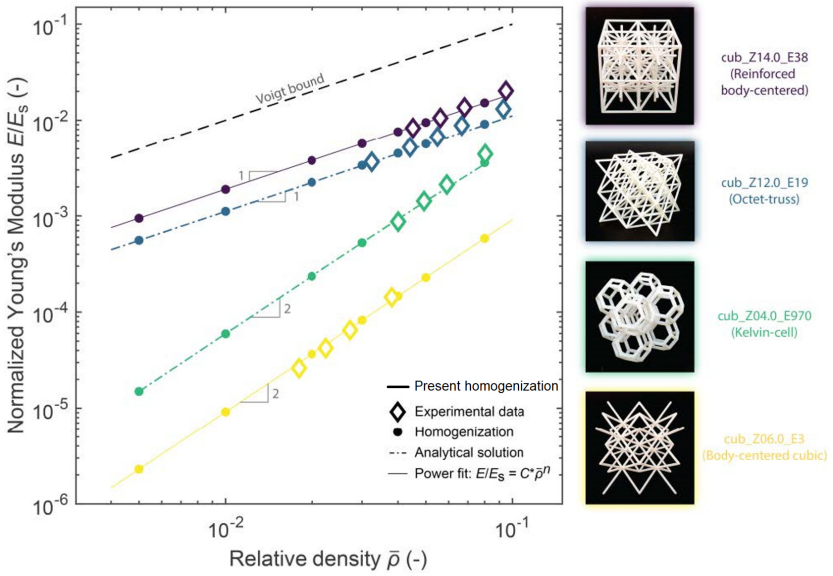

Figure 3: Linear elastic lattices. Scaling behaviour for relative densities $\bar{\rho}$ below 0.1 of the four cell types reinforced body-centred (purple), octet-truss (blue), Kelvin-cell (turquoise), and body-centred cubic (yellow). The solid thick line shows the results obtained via the proposed homogenisation framework. Other results are taken from the literature [4].

it is noticed that, once the $\boldsymbol{e}$-form of the homogenised constitutive law has been computed, alternative forms can be easily derived (Section 2).

6 VALIDATION

The proposed homogenisation procedure has been validated on purely elastic lattice materials. Figure 3 shows the effective Young modulus of four different lattices as a function of the metamaterial relative density. Several analytical, numerical and experimental results taken from the literature are shown. In particular, the well-known linear dependence of the effective Young modulus on the relative density exhibited by stretch-dominated lattices, like the octet-truss, can be recognised. Analogously, the quadratic dependence shown by bending dominated lattices, like the Kelvin cell, appears. The results obtained using the proposed homogenisation method (denoted by a solid thick line) are in reasonable agreement with the reference results.

A repository of more than 17,000 lattices is publicly available in the literature, along with their homogenised material constants, obtained under the assumption of linearly elastic parent material using the Timoshenko beam model [4]. The histograms reported in Figure 4 show the distribution of the relative error of the present solution with respect to the reference one. It can be noticed that the relative error is less than a few per cent. Our model tends to return slightly smaller stiffness moduli, possibly because the exact Saint-Venant model adopted herein tends to be slightly more compliant than the Timoshenko beam model used in [4].

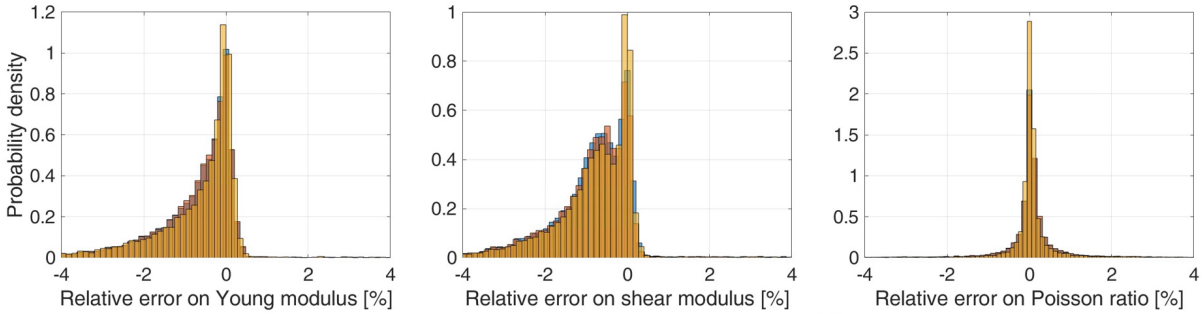

Figure 4: Linear elastic lattices. Histograms of relative errors of results obtained via the proposed homogenisation framework with respect to results taken from the literature [4].

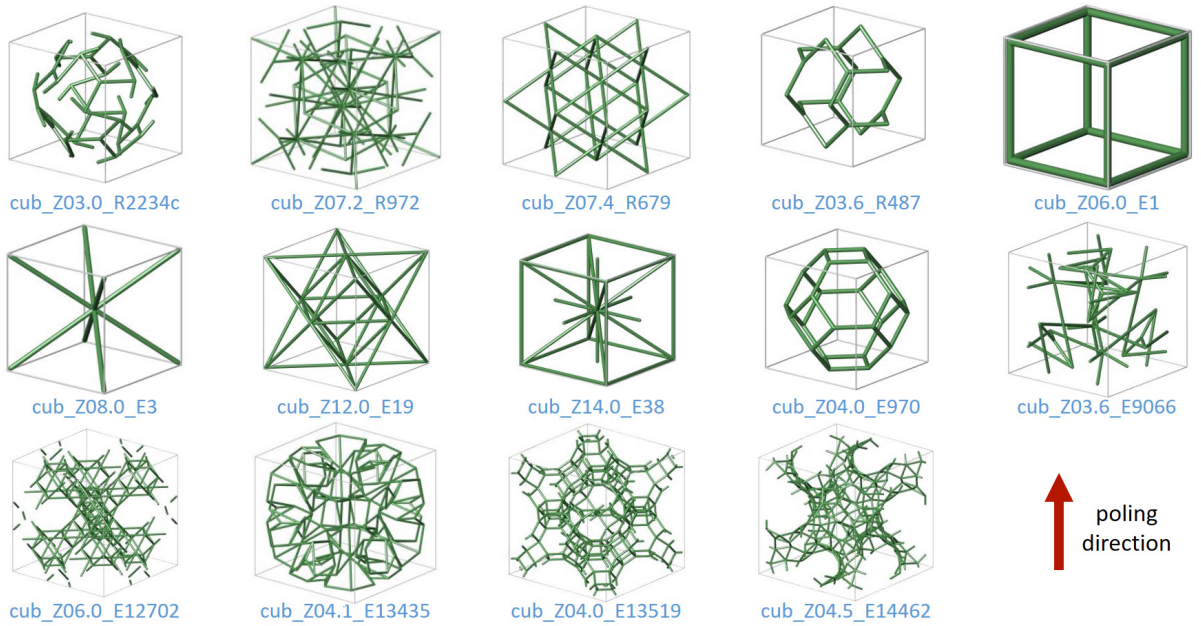

Figure 5: Linear piezoelectric material with vertical poling direction. Periodic unit cells of fourteen lattices [4].

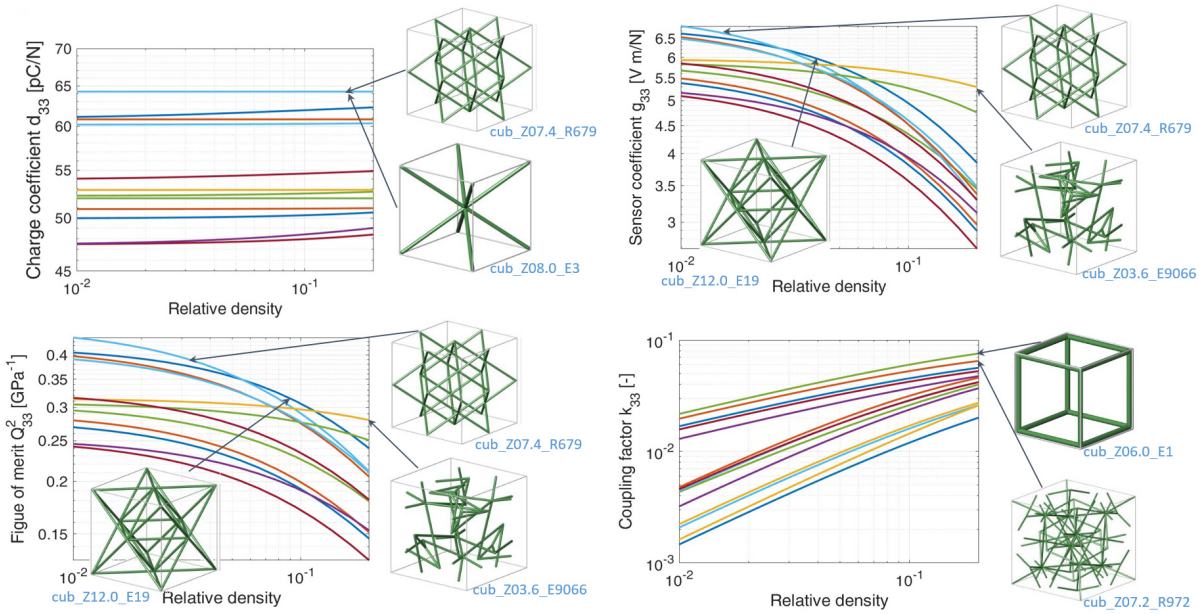

Figure 6: Linear piezoelectric material with vertical poling direction. Charge coefficient d_{33}, voltage coefficient g_{33}, figure of merit Q^2_{33}, coupling factor κ_{33}, computed as a function of the relative density $\bar{\rho}$ of the metamaterial.

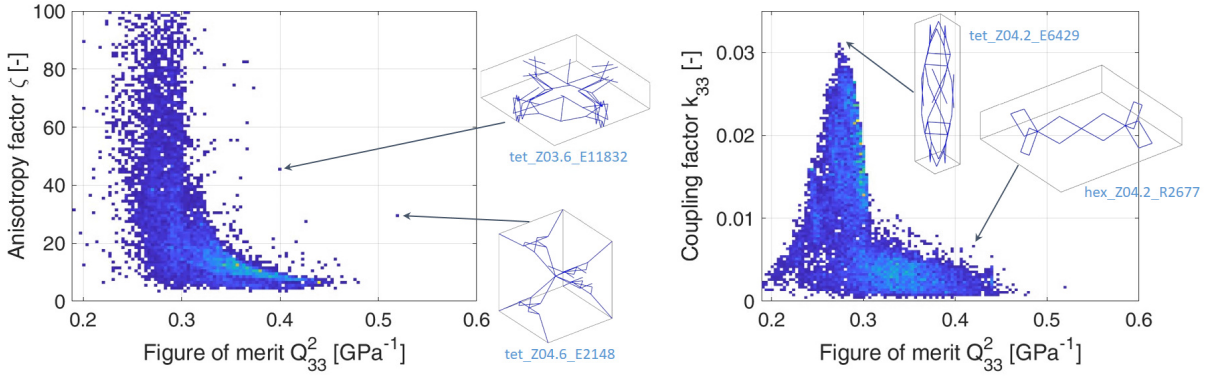

Figure 7: Linear piezoelectric material with vertical poling direction. Anisotropy factor ζ, on the left, and coupling coefficient κ_{33}, on the right, versus Q^2_{33}.

7 RESULTS

Figure 5 shows the periodic unit cells of fourteen lattices. The material is now assumed to be linearly piezoelectric and the poling direction is the vertical one.

For each of those unit cells, the figures of merit introduced in Section 3 have been computed as a function of the relative density of the metamaterial in the rage [0.01–0.2], using the proposed homogenisation approach. The results of the analysis are shown in Figure 6. It can be noticed that the charge coefficient d_{33} is almost invariant with respect to the relative density, whereas the voltage coefficient g_{33} markedly decreases at increasing relative density. The microstructures yielding the highest value of d_{33} or g_{33} are easily identified in each relative-density range. The figure of merit Q_{33}^2, which is the product of d_{33} and g_{33}, has a behaviour very similar to g_{33}. On the other hand, the coupling coefficient κ_{33} has a behaviour similar to the Young modulus, showing a different slope for stretch or bending dominated microstructures.

It is possible to search for unit cell topologies yielding specific combinations of figures of merit. Figure 7 reports the anisotropy factor ζ and the coupling coefficient κ_{33} versus Q_{33}^2. More than 17,000 microstructures [4] have been analysed at a relative density equal to 0.01. Among the achievable combinations, some unit cells exhibiting favourable properties have been pointed out.

8 CONCLUSIONS

A computationally-effective homogenisation method for piezoelectric lattice materials was presented. Instrumental to this method was the solution to the Saint-Venant problem for fully anisotropic piezoelectric beams. The proposed homogenisation method, here applied to a publicly available repository of unit cell topologies, can serve as a tool to identify optimised piezoelectric metamaterials with desired figures of merit. Piezoelectric lattice metamaterials with improved piezoelectric properties may provide cutting-edge technology to improve the application of smart materials significantly. Further studies will account for the finite dimension of nodes in the homogenisation process and will be devoted to gaining insight into the topology-properties relationship of piezoelectric lattice materials.

ACKNOWLEDGEMENTS

The presented work was supported by the Italian Minister of University and Research through the project, "A BRIDGE TO THE FUTURE: Computational methods, innovative applications, experimental validations of new materials and technologies" (No. 2017L7X3CS) within the PRIN 2017 program.

References

[1] Cui, H. *et al.* Three-dimensional printing of piezoelectric materials with designed anisotropy and directional response. *Nat. Mater.* **18**, 234–241 (2019).

[2] Newnham, R. E., Skinner, D. P. & Cross, L. E. Connectivity and piezoelectric-pyroelectric composites. *Mater. Res. Bull.* **13**, 525–536 (1978).

[3] Nodargi, N. A. & Bisegna, P. The saint-venant problem for general anisotropic piezoelectric

cylinders with applications to smart metamaterials design. *Appl. Math. Model.* **93**, 831–851 (2021).

[4] Lumpe, T. S. & Stankovic, T. Exploring the property space of periodic cellular structures based on crystal networks. *Proc. Natl. Acad. Sci. U. S. A.* **118**, e2003504118 (2021).

[5] IEEE Standard on Piezoelectricity. *ANSI/IEEE Std 176-1987* (1988).

[6] Sessler, G. & Hillenbrand, J. Figure of merit of piezoelectret transducers for pulse-echo or transmit-receive systems for airborne ultrasound. *Appl. Phys. Lett.* **103** (2013).

[7] Topolov, V. Y., Isaeva, A. N. & Bisegna, P. Squared figures of merit and electromechanical coupling factors of a novel lead-free 1–3–0 composite for sensor and energy-harvesting applications. *Sens. Actuator A-Phys.* **318**, 112473 (2021).

[8] Ieşan, D. On Saint-Venant's problem. *Arch. Ration. Mech. Anal.* **91**, 363–373 (1986).

[9] Ieşan, D. On Saint-Venant's problem for elastic dielectrics. *J. Elast.* **21**, 101–115 (1989).

[10] Davì, F. Saint-Venant's problem for linear piezoelectric bodies. *J. Elast.* **43**, 227–245 (1996).

[11] Bisegna, P. The Saint-Venant problem for monoclinic piezoelectric cylinders. *Z. Angew. Math. Mech.* **78**, 147–165 (1999).

[12] Bensoussan, A., Lions, J.-L. & Papanicolau, G. *Asymptotic Analysis for Periodic Structures*, vol. 5 of *Studies in Mathematics and Its Applications* (North-Holland, Amsterdam, 1978), 1st edn.

[13] Bisegna, P. & Luciano, R. Variational bounds for the overall properties of piezoelectric composites. *J. Mech. Phys. Solids* **44**, 583–602 (1996).

[14] Bisegna, P. & Luciano, R. On methods for bounding the overall properties of periodic piezoelectric fibrous composites. *J. Mech. Phys. Solids* **45**, 1329–1356 (1997).

[15] Challagulla, K. & Venkatesh, T. Electromechanical response of piezoelectric foams. *Acta Mater.* **60**, 2111–2127 (2012).

[16] Cheng, G.-D., Cai, Y.-W. & Xu, L. Novel implementation of homogenization method to predict effective properties of periodic materials. *Acta Mech. Sin.* **29**, 550–556 (2013).

[17] Lifson, M. L., Kim, M.-W., Greer, J. R. & Kim, B.-J. Enabling simultaneous extreme ultra low-k in stiff, resilient, and thermally stable nano-architected materials. *Nano Letters* **17**, 7737–7743 (2017).